Mantle Melting and Basalt Extraction by Equilibrium Porous Flow

C. C. Lundstrom,* J. Gill, Q. Williams, M. R. Perfit

The chemical composition of mid-ocean ridge basalt, the most prevalent magma type on the planet, reflects the melt's continuous reequilibration with the surrounding mantle during porous flow. Models of basalt extraction that account for the observed uranium-series disequilibria on the Juan de Fuca ridge constrain both the abundance of melt beneath ridges (0.1 to 0.2 percent) and the style of mantle melting. Unlike models that incorporate near-fractional melts (dynamic melting), mixing of equilibrium porous flow melts derived from heterogeneous source materials quantitatively explains the uranium-series observations.

Mid-ocean ridges produce 80% of the annual magmatism on Earth. Recent geochemical data have been used to suggest that mid-ocean ridge basalt (MORB) results from the accumulation and mixing of near-fractional melts produced at different depths in the mantle from homogeneously depleted peridotite (*1*, *2*); however, other data imply that there is significant chemical heterogeneity in the mantle that produces MORB and ubiquitous mixing of melts derived from different sources (*3*).

Distinguishing how MORB is produced through trace- and major-element geochemistry requires assumptions about the elemental composition and degree of mantle heterogeneity before melting. The use of uranium-series (U-series) disequilibria avoids these uncertainties (although assumptions about lithology are still required) because all source materials, regardless of their enriched or depleted character, begin melting in secular equilibrium. Here, we evaluate the ability of different melting models to explain U-series data from the Juan de Fuca (JDF) ridge.

Silicate melts connected at low porosity will move buoyantly relative to their surrounding solid matrix (*4*). Equilibrium melting (or batch melting) has generally referred to the coexistence of a residual solid in chemical equilibrium with all of the melt that it had produced. Because the liquid is able to move, equilibrium melting probably corresponds to continuous reequilibration between moving liquid and the neighboring bulk solid, termed equilibrium porous flow (EPF) (*5*, *6*). For EPF, we use equation 23 of (*6*) that models melts (equivalent to batch melts) that reequilibrate to shallow depths and lose any trace-element signature from garnet-melt partitioning, even if they began their ascent in the garnet peridotite stability field. Alternatively, the melting process could correspond to surface equilibrium during melting, followed by chemical disequilibrium between solid and liquid during transport, referred to as dynamic melting (DM) (*7*–*11*). For DM, we use equation 17 of (*9*) that models mixed polybaric fractional melts that retain trace-element signatures from melting in different parts of the mantle (for instance, a garnet signature from the deepest portions). The question we address with these simple one-dimensional models is whether melts move rapidly from depth in chemical disequilibrium with the surrounding solid (DM), or whether they percolate through and maintain chemical equilibrium with the solid mantle until segregating at shallow depths (EPF).

Both models produce excess daughter isotopes in the magma when the residence time in the melting column of the parent nuclide is longer than that of the daughter (Fig. 1A); that is, when the daughter nuclide is removed more readily from the system than the parent. Thus, even if there is no net fractionation of Th from U at high degrees of melting ($F > 10\%$) as assumed in this modeling, excesses can be produced (*12*). The two models differ in that DM essentially removes all of the Th and U from the solid after only 0.5% melting (*13*). Consequently, excesses of ^{230}Th, ^{226}Ra, and ^{231}Pa are only created during differential movement of melt and solid during the initial stages of melting. In contrast, the continuous interaction of solid and melt in EPF allows small differences in partition coefficients to be exploited over the whole melting column and thus creates larger differences in residence time than does DM at a fixed solid upwelling rate. The EPF model creates excesses throughout the melting column (Fig. 1B); the straight lines for the DM model in Fig. 1B represent the simple assumption (unrealistic for ^{226}Ra) of instantaneous transport. Chemical equilibration with spinel lherzolite, where $D_{\mathrm{Th}}/D_{\mathrm{U}} > 1$ (D is the partition coefficient), does not preclude ^{230}Th excesses from occurring (*6*, *14*). Because all of the U and Th have been transferred from the solid to the melt when it enters the spinel peridotite field, the reversal in Th-U partitioning that occurs has little effect on the ^{230}Th excess already produced.

Mixing processes can mask source heterogeneity. The end result of efficient mixing of chemically distinct melts produced from heterogeneous source materials is difficult to distinguish from that produced by uniform melting of a homogeneous source. Primitive MORB (MgO > 9.5 weight %) with depleted trace-element signatures can be found in tectonic environments less affected by mixing, such as leaky transform faults or off-axis seamounts (*3*). Normal MORB may result from the mixing of a large amount of this depleted basalt with 1 to 5% of an enriched component (*3*). Although mixing affects all elements, it is most apparent in ratios of incompatible elements, and U-series disequilibria should also be affected by mixing.

The U-series disequilibria for specific ridges vary systematically and typically show a negative correlation between (^{230}Th)/(^{232}Th) (activity ratios) and Th/U concentrations (*15*, *16*). (^{226}Ra)/(^{230}Th) and (^{231}Pa)/(^{235}U) also vary as a function of Th/U (*17*, *18*). Our results on recently erupted samples from the New Mounds site (*19*) (Table 1), combined with previous thermal ionization mass spectometry (TIMS) measurements (*16*–*18*), reveal linear trends on the JDF ridge (Fig. 2, A to C), which yield three principal observations. First, mixing plays a critical role in producing the observed disequilibria, which means that end members have petrogenetic rather than temporal significance. Because of the wide range of excesses within ridge segments, averaging disequilibria values grossly oversimplifies the U-series data [see, for example, (*9*, *13*)]. Second, the end members correspond to enriched basalt (Endeavour-like), with higher Th/U, (^{231}Pa)/(^{235}U), and (^{230}Th)/(^{238}U) but lower (^{226}Ra)/(^{230}Th), and more depleted basalt (New Mounds–like) having the opposite properties. Third, as Th/U is an indicator of source heterogeneity (*20*), the degree of source enrichment influences excess ^{230}Th, ^{231}Pa, and ^{226}Ra production.

Our results imply a substantial difference in the melting process for enriched and depleted sources. The range in ^{230}Th excess (9 to 38%) cannot be explained by melting a lithologically homogeneous mantle in either model; variation in the garnet mode is required. The enriched melt may come from a trace element–rich pod or vein, although its lithology (possibly garnet pyroxenite) and melting behavior are uncertain (*21*). In EPF models where melting commences at a greater depth with more garnet, ^{230}Th and

---

C. C. Lundstrom, J. Gill, Q. Williams, Earth Sciences Board, University of California, Santa Cruz, CA 95064, USA.
M. R. Perfit, Department of Geology, University of Florida, Gainesville, FL 32611, USA.

*To whom correspondence should be addressed.

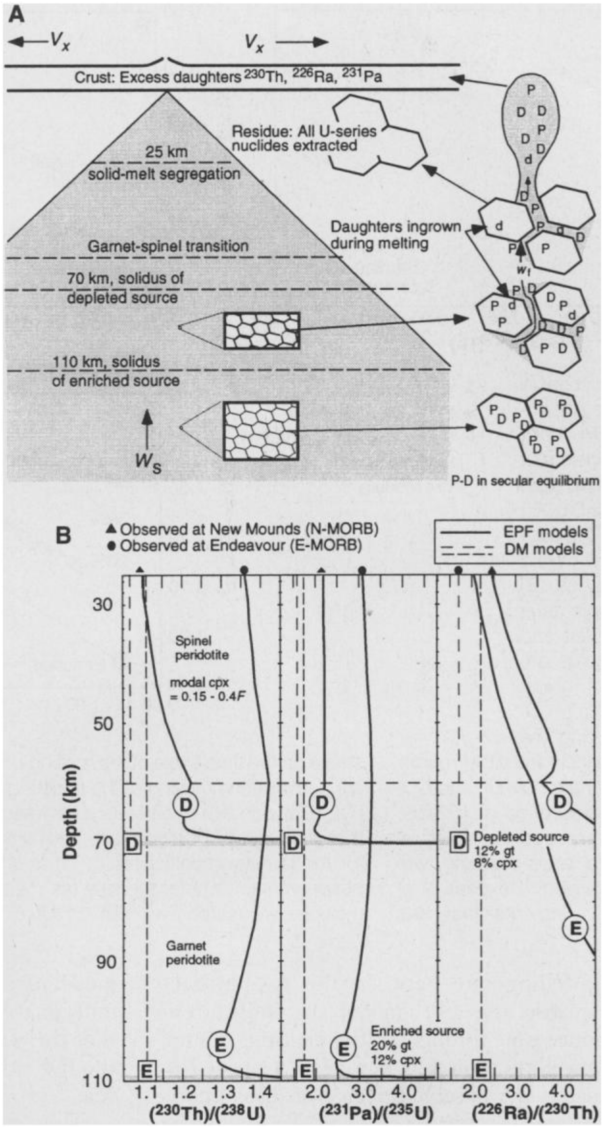

Fig. 1. (**A**) Schematic of U-series excess production during melting. As lithospheric plates diverge, solid mantle (in secular equilibrium for the U-series nuclides) upwells and begins to melt at either 110 or 70 km depending on the source fertility. The connected melt migrates relative to the solid as shown on the right, producing preferential partitioning of the parent (P; for instance, uranium) into the solid over the daughter (D). While P resides in the slowly moving solid, some will decay producing "ingrown" daughter (d). Eventually, all of the U-series nuclides are extracted into the melt, resulting in excess daughter in the erupted basalts. Continuous equilibration with the solid in an EPF model creates excesses throughout the melting column. If the porosity is small (10^{-3}), DM corresponds closely to a near-fractional model, as incompatible elements are quickly removed from the solid (U and Th within the first 0.5% melting) and transported in chemical disequilibrium to the surface with U-series excesses created only during this initial phase of melting. There is no simple intermediate between EPF and DM because partial chemical equilibration (probably diffusionally controlled) during percolation will effectively lessen the liquid-solid partition coefficients, which in turn will require even smaller porosities to produce the observed disequilibria. V_x, half-spreading rate; W_s, solid upwelling rate. (**B**) Parent-daughter excesses as a function of depth in the melting column. The following parameters were used: $W_s = 0.025$ m year^{-1}; ϕ_{max} (maximum porosity) = 0.15%; and partition coefficients $^{gt/l}D_U = 0.015$ and $^{gt/l}D_{Th} = 0.0015$ (*11*), $^{gt/l}D_{Pa} = 6.7 \times 10^{-4}$, $^{cpx/l}D_U = 0.01$, $^{cpx/l}D_{Th} = 0.015$, and $^{cpx/l}D_{Pa} = 6.7 \times 10^{-4}$ (*5*) (where gt/l indicates partitioning between garnet and liquid and cpx/l partitioning between clinopyroxene and liquid). The bulk D_{Ra} was assumed to be 1×10^{-5} everywhere. D and E refer to calculations with a depleted and enriched source, respectively, with melt segregation occurring at a depth of 25 km (*30*). In both melting models (although not shown for DM because of scale), there is an abrupt increase in excess on initial melting, followed by a return toward equilibrium as the parent partitions into the melt. All disequilibria for the DM model are created in the shaded areas (for the enriched and depleted sources, respectively).

^{231}Pa excesses are shifted upward to the observed disequilibria at Endeavour (Fig. 2B). A depth of 110 km and a garnet mode of 20% provide an excellent fit to the data, but other combinations with the EPF model could also work. Considering the complexities involved, this simple model appears to provide robust insights into the process of melt generation (*22*). Furthermore, we do not constrain the crustal production rate, as this depends on assumptions about the U concentration of the enriched and depleted source materials (*23*). Although increasing the garnet mode (but not the depth of melting) produces a greater ^{230}Th excess with DM for the enriched end member, the magnitude of the shift is insufficient to explain the variation observed. Even if the garnet mode is increased to 50%, the dynamic model cannot match the observed range of ^{230}Th excesses (VF in Fig. 2B). In addition, this higher garnet mode in the DM model is more difficult to reconcile with the lack of a strong garnet signature in MORB rare earth element patterns. In the EPF model, reequilibration of the melt with spinel lherzolite erases garnet-derived melt signatures. Because DM models produce more excess ^{230}Th with slower upwelling rates, we have allowed these rates to vary by an order of magnitude (Fig. 2); the continued lack of accord with either the qualitative trends or the quantitative amounts of the observed disequilibria indicates that the DM models cannot reconcile the U-series observations.

There are several reasons for favoring EPF over DM. Although the interpretation of (^{226}Ra)/(^{230}Th) is most susceptible to age uncertainty (*24*), the EPF model matches the observed trend (Fig. 2A) because the clinopyroxene mode, and therefore excess ^{226}Ra, decreases with the higher degrees of melting (F) experienced by the enriched source material. Excess ^{226}Ra is created by EPF in the upper 20 km of the melting column (*6*), whereas DM produces excess only at melt initiation, requiring rapid transport of melt to the surface at velocities of ~100 m year^{-1}. Furthermore, changes in source enrichment (garnet mode) or the solid upwelling rate in DM produce slopes opposite of those observed (Fig. 2A).

The relation between the ^{230}Th excess and the ^{231}Pa excess places the strongest constraint on the melting process (Fig. 2B). EPF with differences in the depth of melt initiation replicates the observed relation between (^{230}Th)/(^{238}U) and (^{231}Pa)/(^{235}U) (*5*). The very large observed excesses in (^{231}Pa)/(^{235}U) are quantitatively matched because equilibrium percolation after U is removed from the solid increases the difference in residence time between U and Pa, an effect that cannot occur during the disequilibrium transport of the DM model. (^{230}Th)/(^{238}U) and (^{231}Pa)/(^{235}U) ratios predict melting rates that differ by more than an order of magnitude for the two systems in DM models (*9*, *13*). This inconsistency is difficult to rationalize because both ^{230}Th and ^{231}Pa are daughters of uranium isotopes, and it is the partition coefficient of the parent that principally controls the magnitude of the disequilibria (*7*). The excellent agreement between the ^{231}Pa and ^{230}Th dating methods for MORB (*16*, *17*), in spite of the differences in the assumptions of initial excess (*25*), further indicates that much of the interridge variation results from mixing. The consistency in dates also indicates that the ^{226}Ra mixing trend (Fig. 2A) could be used to date samples on a fine time scale (*26*).

Variations in the zero age ^{230}Th/^{238}U as a function of Th/U for a single ridge (in places, single segments) must also be explained. Changes in the depth of melt initiation within an EPF model can produce this variation. Such changes are consistent with the petrologic expectation that more enriched materials intersect their solidi at greater depths and thus will form the first melts. For DM, changes in the garnet mode

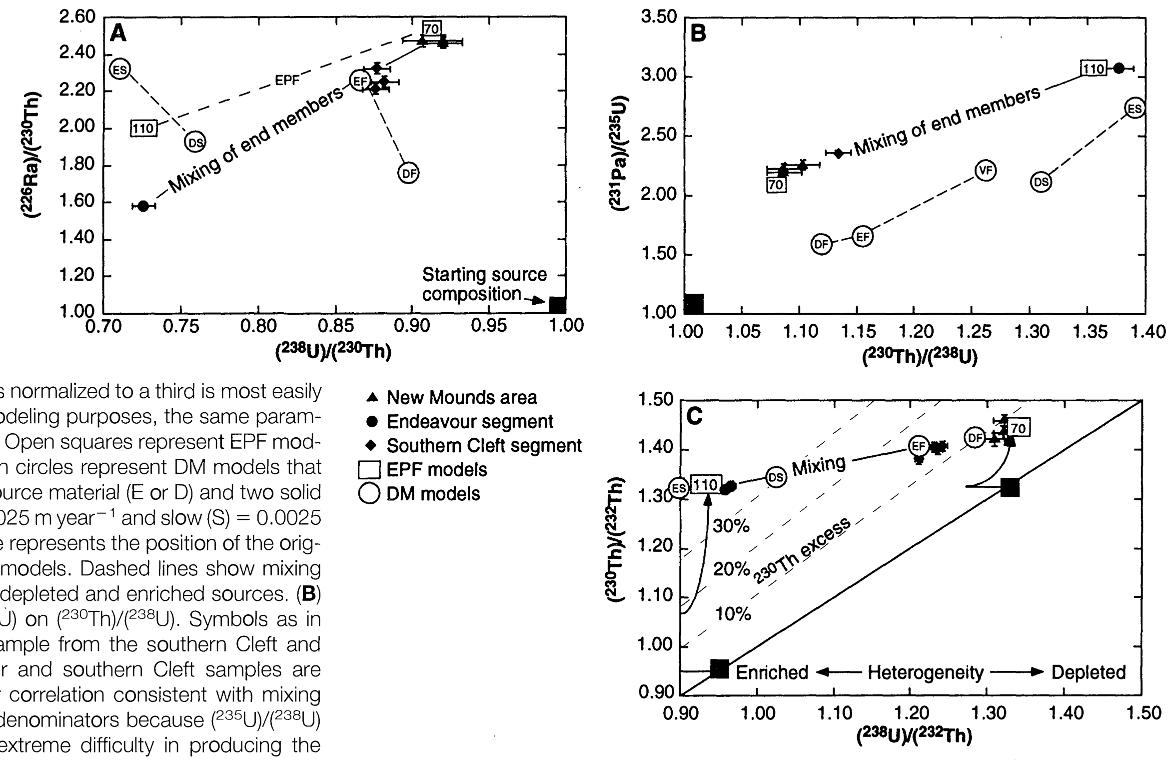

Fig. 2. (**A**) Dependence of (^{226}Ra)/(^{230}Th) on (^{238}U)/(^{230}Th) for Juan de Fuca ridge samples determined with the highest (^{226}Ra)/(^{230}Th) found for the southern Cleft and Endeavour segments (*18*). The use of the highest observed disequilibria minimizes the effect of decay occurring after eruption although there is no precise age constraint on these samples. The linear trend between two trace elements normalized to a third is most easily explained by mixing. For modeling purposes, the same parameters were used as in Fig. 1. Open squares represent EPF models at 110 and 70 km. Open circles represent DM models that use enriched or depleted source material (E or D) and two solid upwelling rates [fast (F) = 0.025 m year^{-1} and slow (S) = 0.0025 m year^{-1}]. The black square represents the position of the original equilibrium state for all models. Dashed lines show mixing trends between melts from depleted and enriched sources. (**B**) Dependence of (^{231}Pa)/(^{235}U) on (^{230}Th)/(^{238}U). Symbols as in (A). (^{231}Pa)/(^{235}U) for the sample from the southern Cleft and (^{230}Th)/(^{238}U) for Endeavour and southern Cleft samples are from (*16*) and (*17*). A linear correlation consistent with mixing exists despite the different denominators because (^{235}U)/(^{238}U) is constant. To show the extreme difficulty in producing the magnitude of these excesses in the DM model, we have included a DM model calculation (shown with a VF) in which extreme values for the bulk D_U and D_{Th} (0.008 and 0.0036, respectively) were used. (**C**) Dependence of (^{230}Th)/(^{232}Th) on (^{238}U)/(^{232}Th). (^{230}Th)/(^{238}U) for Endeavour and southern Cleft is from (*16*). In contrast to (A) and (B), which incorporate ratios involving two nuclides produced during the melting process, (C) shows the excess of a nuclide, ^{230}Th, as a function of the ratio of two elements that are stable on the time scale of the melting process, ^{232}Th and ^{238}U. The evolutionary paths during melting of the enriched and depleted melts corresponding to Fig. 1B are shown. A difference between Th/U$_{melt}$ and Th/U$_{source}$ is unlikely for the total degree of melting assumed for MORB (F >10%) given the small values for the partition coefficients of Th and U. This implies a systematic relation between source heterogeneity (as measured by Th/U) and how the mantle melts [as measured by (^{230}Th)/(^{238}U), (^{226}Ra)/(^{230}Th), and (^{231}Pa)/(^{235}U)].

cannot account for the observed range in ^{230}Th excess. Although a variable melting rate (or solid upwelling rate) could account for the range, it is not clear whether the solid upwelling (or melting) rate can vary by an order of magnitude or be so strongly related to heterogeneity (Fig. 2C).

Finally, there is a difference in the solid upwelling rate between the two models. Because the EPF model maximizes residence time throughout the melting column, upwelling rates (25 mm year^{-1}) needed to match the observed degree of disequilibria (*6*) are tectonically realistic. To match the higher ^{230}Th and ^{231}Pa disequilibria observed in the Endeavour basalts, the DM model requires solid upwelling rates of ~2.5 mm year^{-1}. Such slow upwelling implies that the width of the upwelling area under the JDF ridge [half-spreading rate of ~3 cm year^{-1} (*16, 27*)] would be ~1500 km.

That the U-series disequilibria require low-porosity melting of depleted mantle as well as low-porosity melting of enriched

Table 1. U-series data from the Juan de Fuca ridge. Errors given for ^{230}Th, ^{231}Pa, and ^{226}Ra reflect the internal precision of an individual measurement. On the basis of the reproducibility of Th and U concentration measurements [in parts per billion (ppb)] of MORB, we estimated our uncertainty on (^{238}U)/(^{232}Th) to be ±1.5%. Spike calibrations were verified by measurement of the rock standard Table Mountain latite (TML) (jar 2). The number of measurements for all TML values was six except for (^{226}Ra) and (^{226}Ra)/(^{230}Th) (n = 7) and (^{231}Pa) and (^{231}Pa)/(^{235}U) (n = 1). The radioactive decay constants were as follows: $\lambda_{230} = 9.195 \times 10^{-6}$ year^{-1}, $\lambda_{226} = 4.326 \times 10^{-4}$ year^{-1}, $\lambda_{231} = 2.116 \times 10^{-5}$ year^{-1}.

Sample (lattitude)	Th (ppb)	U (ppb)	Th/U	(^{238}U)/(^{232}Th)	(^{230}Th)/(^{232}Th)	(^{230}Th)/(^{238}U)	(^{234}U)/(^{238}U)	(^{226}Ra) (dpm/g)	(^{226}Ra)/(^{230}Th)	(^{231}Pa) 10^3 (dpm/g)	(^{231}Pa)/(^{235}U)
A2430-4 (45° 08.0′)	193.8 189.8 190.6	83.2 81.0 83.9	2.314	1.320	1.44 ± 1	1.087	1.012 0.998	0.165 ± 3 0.164 ± 3	2.46	6.12 ± 6	2.20 ± 2
A2262-4 (45° 00.5′)	176.4 179.5 178.1	76.7 76.5 75.5	2.335	1.309	1.42 ± 1	1.086	1.001 1.001	0.152 ± 3	2.46	6.11 ± 24 5.87 ± 11	2.32 ± 9 2.23 ± 4
A2269-2 (44° 59.0′)	200.3	86.6	2.313	1.321	1.46 ± 1 1.47 ± 2 1.43 ± 3	1.103	0.993	0.176 ± 1 0.176 ± 1 0.175 ± 3	2.47	6.72 ± 13	2.26 ± 4
TT175-17-23 (47° 54.4′)		104†								10.94 ± 8	3.06 ± 2
TML	31.1	11.0	2.827	1.081	1.084	1.003	1.002	8.12	0.996	341	1.000 ± 8

*Refer to (*19*) for further information on all samples except for TT175-17-23 [see (*20*)] and TML. †From (*16*).

pods is shown by the $(^{226}\text{Ra})/(^{230}\text{Th})$ results (Fig. 2A). These data constrain the porosity to be <0.2% and demonstrate that the greatest $(^{226}\text{Ra})/(^{230}\text{Th})$ is found within the most depleted samples. Thus, it appears that both depleted and enriched end members are produced by percolative flow through a low-porosity matrix, rather than the observed disequilibria simply reflecting the mixing domination of enriched melts over melts from depleted mantle.

Calculations have suggested that melts might not be able to maintain chemical equilibrium at the small porosities and high melt velocity mandated by EPF (*28*). These calculations consider that solid-state diffusion is the sole mechanism for equilibrating melt with solid. Alternatively, dissolution and reprecipitation might be the dominant mechanism by which melts reequilibrate. Our model suggests that large differences in composition and the pressure of melt initiation exist between melts, making dissolution and reprecipitation an attractive means for establishing equilibrium. Indeed, this mechanism, which is experimentally poorly constrained, could allow both high fluid velocities (~1 to 5 m year^{-1}) and small porosities. Melt distributions in peridotites under differential stress show evidence for grain-scale flow and indicate that melts tend to cover grain boundaries in deforming regimes such as beneath mid-ocean ridges (*29*).

If equilibrium melting controls U-series disequilibria in MORB, the implications are profound. Differential movement of melt and solid at porosities on the order of 10^{-3} is required, and this small porosity must be maintained throughout the melting region. Because the ^{230}Th disequilibria cannot be created within the spinel peridotite field, melt velocities must be meters per year, indicating that the permeability must be extremely high for this low porosity. Mass conservation requires this rapid melt velocity given the porosity, degree of melting, and solid upwelling rate (*30*). Also, this low porosity would be difficult to image seismically. Observations of high seismic attenuation beneath ridges suggest that either this small amount of melt greatly influences the seismic attenuation or that much of the attenuation observed under ridges is purely thermal in origin (*31*).

We have shown that the U-series data strongly suggest that MORBs are produced by EPF in which the chemical signature of the melt is generated at the last, shallowest point of equilibration with the mantle. This conclusion conflicts with previous data and modeling, which were interpreted to indicate that near-fractional melting (*1*, *2*) produces MORB. Our data and modeling are independent of assumptions about mantle source composition and heterogeneity and, when coupled with our ability to model three parent-daughter pairs, render EPF the most tractable mechanism for MORB petrogenesis.

REFERENCES AND NOTES

1. K. T. M. Johnson and H. J. B. Dick, *J. Geophys. Res.* **97**, 9219 (1992); A. V. Sobolev and N. Shimizu, *Nature* **363**, 151 (1993); K. Ross and D. Elthon, *ibid.* **365**, 826 (1993); S. R. Hart, *Proc. Natl. Acad. Sci. U.S.A.* **90**, 11914 (1993); D. McKenzie and M. J. Bickle, *J. Petrol.* **29**, 625 (1989); K. T. M. Johnson, H. J. B. Dick, N. Shimizu, *J. Geophys. Res.* **95**, 2661 (1990).
2. C. H. Langmuir, E. M. Klein, T. Plank, in *Mantle Flow and Melt Generation at Mid-Ocean Ridges* (American Geophysical Union, Washington, DC, 1992), pp. 183–280.
3. J. H. Natland, in *Magmatism in the Ocean Basins*, A. D. Saunders and M. J. Norry, Eds. (Blackwell Scientific, Oxford, 1989), pp. 41–70; R. Hekinian, D. Bideau, R. Hebert, Y. Niu, *J. Geophys. Res.* **100**, 10163 (1995); D. J. Fornari *et al.*, *Earth Planet. Sci. Lett.* **89**, 63 (1988).
4. H. S. Waff and J. R. Bulau, *J. Geophys. Res.* **84**, 6109 (1979); D. L. Kohlstedt, in (*2*), pp. 103–121.
5. C. C. Lundstrom *et al.*, *Earth Planet. Sci. Lett.* **128**, 407 (1994).
6. M. Spiegelman and T. Elliott, *ibid.* **118**, 1 (1993).
7. D. McKenzie, *ibid.* **74**, 81 (1985).
8. R. W. Williams and J. Gill, *Geochim. Cosmochim. Acta* **53**, 1607 (1989).
9. C. Richardson and D. McKenzie, *Earth Planet. Sci. Lett.* **128**, 425 (1994).
10. P. D. Beattie, *Nature* **363**, 63 (1993).
11. T. Z. LaTourrette, A. K. Kennedy, G. J. Wasserburg, *Science* **261**, 739 (1993).
12. This interpretation contrasts with a recent explanation for ^{230}Th excesses in Hawaii through crystal-liquid Th-U fractionation alone; K. W. Sims *et al.*, *Science* **267**, 508 (1995). By using a modification of their equation 1 for Th and U. With the enriched-source partition coefficients of Fig. 1 and a value for F of 0.1, the fractionation of Th from U (αTh/U) is 1.018; this is almost within the uncertainty of the measurement. See also R. K. O'Nions and D. McKenzie, *Philos. Trans. R. Soc. London* **342**, 65 (1993).
13. H. Iwamori, *Earth Planet. Sci. Lett.* **125**, 1 (1994).
14. Higher ^{230}Th excesses result from increased depth for two reasons. First, the longer time in contact with garnet increases the residence time differences between ^{230}Th and ^{238}U. Second, flux balance requires that $\rho_s W_s F = \rho_f \phi w_f$, where W_s and w_f are the solid and melt velocities, respectively, F is the total degree of melting, ϕ is the porosity, and ρ_s and ρ_f are the solid and liquid densities (3300 kg/m^3 and 2800 kg/m^3, respectively). Because F is greater in the enriched materials (but W_s and ϕ are constant), w_f is higher for the enriched melt resulting in less decay during transport through spinel lherzolite.
15. I. Reinitz and K. K. Turekian, *Earth Planet. Sci. Lett.* **94**, 199 (1989).
16. S. J. Goldstein, M. T. Murrell, D. R. Janecky, J. R. Delaney, D. A. Clague, *ibid.* **107**, 25 (1991).
17. S. J. Goldstein, M. T. Murrell, R. W. Williams, *ibid.* **115**, 151 (1993).
18. A. M. Volpe and S. J. Goldstein, *Geochim. Cosmochim. Acta* **57**, 1233 (1993).
19. M. C. Smith, M. R. Perfit, I. R. Jonasson, *J. Geophys. Res.* **99**, 4787 (1994). Two of these samples are age-constrained by repeat sea-beam surveys to have been erupted after 1981 [W. W. Chadwick, R. W. Embley, C. G. Fox, *Nature* **350**, 4168 (1991)], whereas the third sample, which appears visibly fresh, comes from a pillow just southeast of New Mounds. Samples were hand-picked glasses that were leached with established procedures (*15*, *18*). All analyses except ^{231}Pa were performed on a VG 54-30 mass spectrometer at the University of California, Santa Cruz (UCSC). ^{231}Pa analyses were performed on an NBS 1260 mass spectrometer at UCSC. Both instruments are equipped with ion counters whose linearity has been verified by repeated measurements on NBS standard U-010.
20. The basalts from Endeavour have been described as E-MORBs (enriched) [J. L. Karsten, J. R. Delaney, J. M. Rhodes, R. A. Liias *J. Geophys. Res.* **95**, 19235 (1990)] on the basis of their Zr/Y and Zr/Nb ratios.
21. C. J. Allegre and D. L. Turcotte, *Nature* **323**, 123 (1986); D. Ben Othman and C. J. Allegre, *Earth Planet. Sci. Lett.* **98**, 129 (1990). We have assumed a constant melting rate of 0.4% per kilometer for both source materials, although there is considerable uncertainty about pyroxenite melting rates. A case could be made for either slower melting rates at melt initiation (*9*) or faster rates due to higher H_2O content. If a slower melting rate were used, the DM model for the enriched melt in Fig. 2B would move outward along a vector from EF to ES and beyond (Fig. 2B).
22. The actual time of contact between the melt and the enriched source introduces some uncertainty. The EPF model treats the problem as continuous interaction throughout a depth range with a uniformly higher garnet mode, although the high velocity of melt relative to the solid would quickly separate melt from heterogeneously distributed enriched solid. However, our approach also applies to reactive flow where enriched melt interacts with unmelted peridotite to precipitate garnet and clinopyroxene during percolation. In a sense, we are assessing how residence time differences affect the relations between excesses in the two models.
23. It is likely that the U concentration of the enriched source greatly exceeds that of the depleted source; thus, only 1 to 5% of enriched melt by volume could create the observed range in disequilibria. Melting of depleted peridotite would then dominate crustal production.
24. The half-life of ^{226}Ra is 1600 years. Not only could significant decay occur after eruption and before collection, but there could also be significant decay during any transport from the last point of solid-liquid equilibration (which includes storage time in magma chambers).
25. The ^{230}Th dating method is based on the assumption of constant $(^{230}\text{Th})/(^{232}\text{Th})$ on eruption for basalts of a similar composition. The ^{231}Pa dating method is based on the assumption of constant $(^{231}\text{Pa}/^{235}\text{U})$ (disequilibria) on eruption for chemically similar basalts.
26. This approach differs from previously suggested methods of dating using ^{226}Ra excess; K. H. Rubin and J. D. McDougall, *Earth Planet. Sci. Lett.* **101**, 313 (1990).
27. The differences in the solid upwelling rates are based on the assumption of constant melting rate. The flux of the plate away from the axis must approximate the flux of the upwelling mantle replacing it. Therefore, width = $V_x d/W_s$, where V_x is the half-spreading rate and d is depth.
28. M. Spiegelman and P. Kenyon, *Earth Planet. Sci. Lett.* **109**, 611 (1992).
29. Z. Jin, H. W. Green, Y. Zhou, *Nature* **372**, 164 (1995).
30. The variable w_f can be calculated from $\rho_s W_s F = \rho_f \phi w_f$. If W_s is 0.025 m year^{-1}, F is 0.20, and ϕ is constrained to be ~0.0015 by the presence of U-series excess, then $w_f = 3.9$ m year^{-1}. Simple Darcy's law analysis suggests that this velocity is reasonable: if $w_f = a^2 \phi^{n-1} \Delta\rho g/\eta C$ [equation 15 of (*9*)] with a (grain size) = 0.002 m, $n = 2$, $\Delta\rho g = 5000$ kg $\text{m}^{-2}\ \text{s}^{-2}$, η (viscosity) = 1 Pa · s, and C [constant from (*9*)] = 100, then w_f is 9.4 m year^{-1}. The time taken for percolation from a depth of 60 km (the last point at which $D_{Th}/D_U < 1$) to segregation at a depth of 25 km [major elements require at least this depth of segregation [P. C. Hess, in (*2*), pp. 67–102] at 3.9 m year^{-1} would be less than 10,000 years, or only 1/7 of the half-life of ^{230}Th (75,000 years).
31. H. Sato, I. S. Sacks, T. Murase, G. Muncill, H. Fukuyama, *J. Geophys. Res.* **94**, 10647 (1989).
32. We thank J. Delaney and V. Robigou for donating sample TT175-17-23 for ^{231}Pa analysis; Z. Palacz, D. Sampson, and W. Schillinger for technical support; and F. Hochstaedter, K. Rubin, and two anonymous reviewers for helpful comments. C.C.L., J.B.G., and Q.W. were supported by NSF and IGPP-LLNL. M.R.P. and collection of the southern JDF samples by ALVIN were supported by NSF grants OCE 8716827 and OCE 8918890.

8 June 1995; accepted 21 September 1995